Bioorganic & Medicinal Chemistry 18 (2010) 3361–3370

Contents lists available at ScienceDirect

Bioorganic & Medicinal Chemistry

journal homepage: www.elsevier.com/locate/bmc

Mechanism of influence of phosphorylation on serine 124 on a decrease of catalytic activity of human thymidylate synthase

Adam Jarmuła [a,*], Tomasz Frączyk [a], Piotr Cieplak [b], Wojciech Rode [a]

[a] Nencki Institute of Experimental Biology, Polish Academy of Sciences, 3 Pasteur St., 02-093 Warszawa, Poland
[b] The Burnham Institute for Medical Research, 10901 N. Torrey Pines Road, La Jolla, CA 92037, USA

ARTICLE INFO

Article history:
Received 5 January 2010
Revised 1 April 2010
Accepted 6 April 2010
Available online 9 April 2010

Keywords:
Thymidylate synthase
Serine phosphorylation
Molecular dynamics
Essential dynamics
MM-GBSA

ABSTRACT

Regulation by phosphorylation is a well-established mechanism for controlling biological activity of proteins. Recently, phosphorylation of serine 124 in human thymidylate synthase (hTS) has been shown to lower the catalytic activity of the enzyme. To clarify a possible mechanism of the observed influence, molecular dynamics (MD), essential dynamics (ED) and MM-GBSA studies were undertaken. Structures derived from the MD trajectories reveal incorrect binding alignment between the pyrimidine ring of the substrate, dUMP, and the pterine ring of the cofactor analogue, THF, in the active site of the phosphorylated enzyme. The ED analysis indicates changes in the behavior of collective motions in the phosphorylated enzyme, suggesting that the formation of the closed ternary complex is hindered. Computed free energies, in agreement with structural analysis, predict that the binding of dUMP and THF to hTS is favored in the native compared to phosphorylated state of the enzyme. The paper describes at the structural level how phosphorylation at the distant site influences the ligand binding. We propose that the 'phosphorylation effect' is transmitted from the outside loop of Ser 124 into the active site via a subtle mechanism initiated by the long-range electrostatic repulsion between the phosphate groups of dUMP and Ser124. The mechanism can be described in terms of the interplay between the two groups of amino acids: the link (residues 125–134) and the patch (residues 189–192), resulting in the change of orientation of the pyrimidine ring of dUMP, which, in turn, prevents the correct alignment between the latter ring and the pterin ring of THF.

1. Introduction

Thymidylate synthase (TS; EC 2.1.1.45) catalyzes the reductive methylation of deoxyuridine monophosphate (dUMP) by $N^{5,10}$-methylenetetrahydrofolate (meTHF), which leads to the formation of two products: thymidylate (dTMP) and dihydrofolate. As the sole intracellular de novo source of synthesized dTMP,[1] the enzyme is a target in chemotherapy.[2,3] TS has been ascribed also non-catalytic activities, including capacity to bind and repress translation of certain mRNA sequences, and suggested to be a translational regulator of cellular gene expression.[4] Furthermore, the enzyme was recently proposed to possess an oncogene-like activity.[5]

TS was found, in an in vitro study, to be a new substrate for each of the two monomeric catalytic subunit isoforms of human protein kinase CK2, CK2α and CK2α′,[6] with serine residue at position 124 in the human enzyme protein identified by mass spectrometric analysis as the phosphorylation site. There was no change in K_m for either dUMP or meTHF (it was considered likely that the K_m values observed in the experiment characterized active, unmodified enzyme molecules, rather than those phosphorylated), but the enzyme catalytic efficiency, determined as the V^{app}_{max} value, appeared to be lowered by 50% by the modification.[7] The latter pointed to a strong influence of human TS Ser 124 phosphorylation on the enzyme activity, as CK2α used in that experiment was found to be capable to phosphorylate only about 40% of human TS molecules. Of note is that rat, mouse and *Trichinella spiralis* TS proteins are also CK2 substrates. In the *T. spiralis* TS, Tyr 118, an amino acid residue corresponding to human TS Ser 124, has been identified as the most probable site of phosphorylation.[7] As discussed in Frączyk et al.,[7] there seems to be a strong possibility of TS to undergo CK2-catalyzed phosphorylation in vivo, however, definitive experimental evidence of this has yet to be obtained, that is, by an antibody against a (phos)Ser124-containing peptide corresponding to this region of the TS sequence.

In order to learn the structural mechanism responsible for the observed influence of Ser 124 phosphorylation on the enzyme activity of human TS (hTS), molecular modeling studies were

Abbreviations: meTHF, $N^{5,10}$-methylenetetrahydrofolate; TS, thymidylate synthase; hTS, human thymidylate synthase; RMSF, root-mean-square fluctuation; (phos)hTS, phosphorylated hTS; THF, tetrahydrofolate; ED, essential dynamics; MD, molecular dynamics; PDB, protein data bank.

* Corresponding author. Fax: +48 22 8225342.
E-mail address: a.jarmula@nencki.gov.pl (A. Jarmuła).

0968-0896/$ - see front matter © 2010 Elsevier Ltd. All rights reserved.
doi:10.1016/j.bmc.2010.04.019

undertaken. The results indicate that phosphorylation impacts the enzyme activity by affecting the binding of ligands in the active site of hTS.

2. Results and discussion

2.1. RMSD and RMSF

Table 1 presents the RMSDs between various sets of coordinates. These include: RMSD between (i) the average structures from data collection runs and the structures after equilibration (AV w.r.t. EQ), (ii) average structures and the structures after minimization (AV w.r.t MIN), (iii) structures after equilibration and structures after minimization (EQ w.r.t. MIN). The RMSD values in the AV w.r.t. EQ column are smaller than the corresponding values in the EQ w.r.t. MIN column, indicating the duration of the equilibration phases was sufficient to produce more stable trajectories in the data collection phases of the simulations. The same was reflected in the potential and kinetic energies of the systems, converging separately to stable averages before the end of the equilibration periods (not shown). The RMSD values in the AV w.r.t. MIN column are smaller (hTS-dUMP and (phos)hTS-dUMP-THF complexes) or larger ((phos)hTS-dUMP and hTS-dUMP-THF complexes) compared to the corresponding values in the EQ w.r.t. MIN column, indicating a drift of the trajectories from the data collection periods toward (the former case), or away from (the latter case), the coordinates of the systems after minimization. The RMSDs as a function of time over the 2 ns molecular dynamics simulations runs are shown in Figure 1. Simulations of the three of the four simulated systems, hTS-dUMP, (phos)hTS-dUMP and (phos)hTS-dUMP-THF, resulted in stable trajectories throughout the entire respective runs, while the trajectory of the hTS-dUMP-THF system reached a plateau in the 800–2000 ps region. The mean RMSD from these simulations amounted to a moderate range between about 1.4 and 1.8 Å, with a value of 1.37 Å for hTS-dUMP, 1.83 Å for (phos)hTS-dUMP, 1.80 Å for hTS-dUMP-THF, and 1.43 Å for (phos)hTS-dUMP-THF.

Table 1
Backbone RMSD (Å) calculated in different phases of MD simulations

Complex	RMSD		
	EQ w.r.t. MIN	AV w.r.t. EQ	AV w.r.t. MIN
hTS-dUMP	1.36	0.91	1.15
(phos)hTS-dUMP	1.42	0.90	1.68
hTS-dUMP-THF	1.34	1.21	1.66
(phos)hTS-dUMP-THF	1.45	1.05	1.23

EQ, MIN and AV denote: after equilibration, after minimization and average structures, respectively, from the data collection runs.

The average RMSF per residue (Fig. 2) have been calculated from the trajectories of the data collection runs. The largest fluctuations correspond invariantly to surface regions of the enzyme, being in qualitative agreement with the experimental B-factors for the crystal structure of the hTS-dUMP-Tomudex complex[8] (not shown). Overall, the data show relatively similar fluctuation patterns for all systems. However, the phosphorylated systems were, in general, less mobile than the corresponding native systems, undergoing less intense fluctuations in several regions of the protein chain. The latter is reflected in the averages from the residue RMSF, which are equal to 3.14 Å for hTS-dUMP, 3.04 Å for (phos)hTS-dUMP, 3.08 Å for hTS-dUMP-THF, and 2.93 Å for (phos)hTS-dUMP-THF. This effect is especially pronounced in the long peripheral region extending from the asparagine 260 to the C-terminal threonine 306, where the fluctuation peaks reach as high as approx. 4–5 Å in hTS-dUMP and hTS-dUMP-THF, while they are lower by approx. 1–2 Å in (phos)hTS-dUMP and (phos)hTS-dUMP-THF. Another distinct effect is associated with different mobility of residues located in the surface α-helix/loop region (110–131) containing the phosphorylation site, Ser 124. In this region, strong fluctuations with large amplitudes of approx. 4.0–4.5 Å ((phos)hTS-dUMP-THF) are observed in contrast to the magnitude of amplitudes for hTS-dUMP

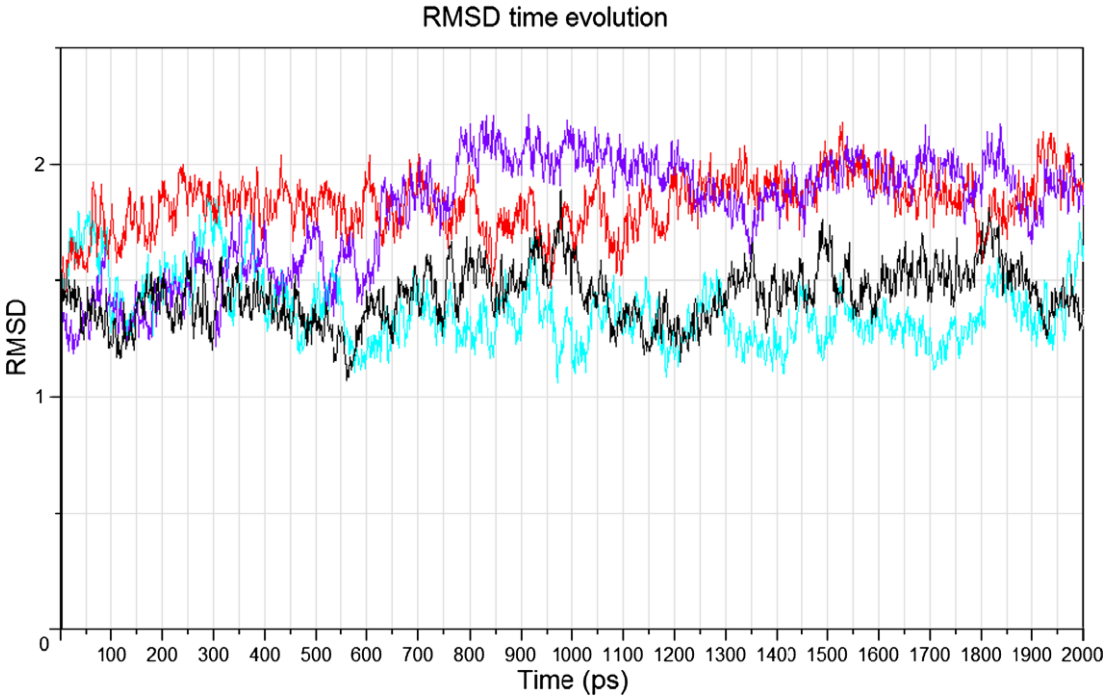

Figure 1. Backbone RMSD (Å) profiles in the courses of the 2000 ps data collection runs (cyan: hTS-dUMP; red: (phos)hTS-dUMP; violet: hTS-dUMP-THF; black: (phos)hTS-dUMP-THF).

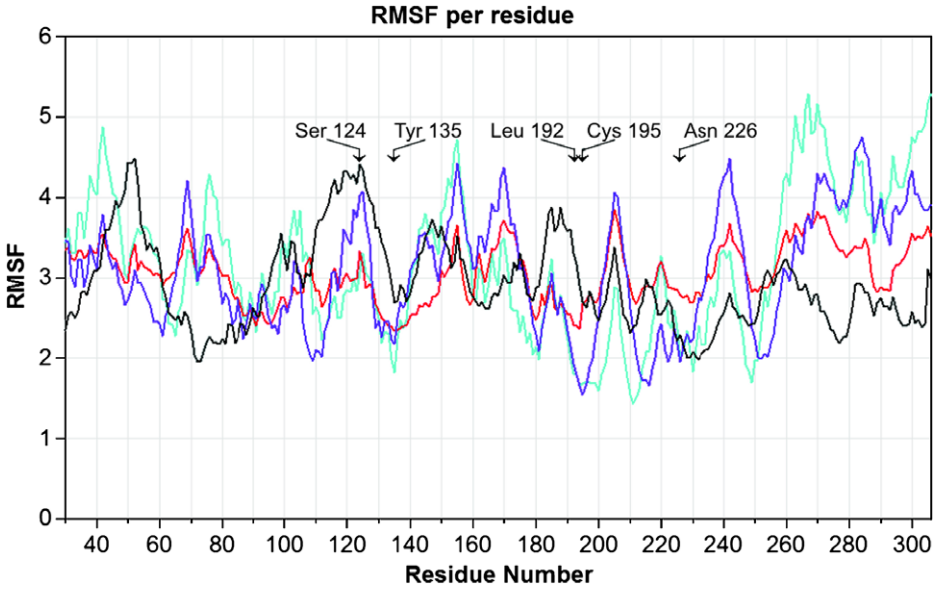

Figure 2. Average per-residue backbone RMSF (Å) in hTS-dUMP (cyan), (phos)hTS-dUMP (red), hTS-dUMP-THF (violet) and (phos)hTS-dUMP-THF (black). Important residues reported explicitly in the text are indicated by arrows.

and (phos)hTS-dUMP (approx. 2.5–3.0 Å) or for sub-region 119–127 of hTS-dUMP-THF (approx. 3.5–4.0 Å). Those results indicate that the mobility of the phosphorylated loop is (i) higher in the ternary compared to binary complexes, and (ii) reaches particularly high values for the (phos) ternary system.

2.2. Essential dynamics

The overall patterns of motions have been analyzed with the essential dynamics (ED) method. There are 6–8 eigenvectors in the simulated systems corresponding to eigenvalues higher than 5 Å^2, which may be considered an approximate lower limit to describe motions of a protein within a reasonable accuracy. The first eigenvectors, characterized by the by-far largest eigenvalues, explain 17.2–31.7% of the total variance in the motions. This number is system dependent. These eigenvectors can be used for comparing dynamics of the simulated systems. Time evolution of trajectories projected on the first eigenvector have been computed and plotted for each pair of the systems, including hTS-dUMP and (phos)hTS-dUMP (pair 1), hTS-dUMP-THF and (phos)hTS-dUMP-THF (pair 2), hTS-dUMP and hTS-dUMP-THF (pair 3), and (phos)-hTS-dUMP and (phos)hTS-dUMP-THF (pair 4); see Figure 3. The calculated correlation coefficients (r^2) of 0.73 (pair 1), 0.77 (pair 2), 0.34 (pair 3) and 0.71 (pair 4) indicate the motions were strongly analogous between the native and phosphorylated (pairs 1 and 2) and between (phos) binary and (phos) ternary (pair 4) systems, whereas poor correlation is observed between the native binary and native ternary (pair 3) systems. These data demonstrate that the dominant motion differs between the native binary and ternary systems, whereas phosphorylation reduces the difference. In addition, the linear regression coefficients of 0.70 (1), 0.67 (2), 0.53 (3) and 0.71 (4) show the motions were suppressed in the phosphorylated compared to native (pairs 1 and 2; in accordance with the RMS fluctuations), and in the ternary relative to binary (pairs 3 and 4), systems. Together, the statistical parameters reveal that phosphorylation on Ser 124 has both suppressing and uniformizing effect on the motions corresponding to the first eigenvector. The dominant motion of each residue in every system studied here is demonstrated in Figure 4. It shows that the dominant movement defined by the first eigenvector is a motion of the region flanking the entrance to the active site pocket: extending to the inside of the pocket at both flanks in the native binary system (Fig. 4A), or at a single flank (on the side of the loop containing Ser 124) in the native ternary system (Fig. 4C). This movement is considerably suppressed at the corresponding flanks in the both phosphorylated systems (Fig. 4, B and D). From the functional point of view, such motions contribute (together with the movement of the C-terminus and overall tightening of the active site)[9,10] to the opening/closing of the active site. Therefore, the ED results suggest that the phosphorylation on Ser 124 may hinder the transition to the closed, active hTS conformation in the process of the covalent ternary complex formation. This reasoning, however, should be taken with caution. In the present study, all the simulations started with the enzyme in the wide-open active site conformation inherited from the crystal structure of the hTS-dUMP-Tomudex complex. Within the present approach it is not possible to model formation of the covalent bond between C(6) of dUMP and the catalytic Cys 195, thus possible transitions to the fully closed conformation could not be expected. Despite this limitation, a clear effect of the narrowing of the active site entrance, suggestive of a conformational change toward the closed form of the active site, can be observed in the native ternary complex, hTS-dUMP-THF. Interestingly, this effect is suppressed in the (phos)hTS-dUMP-THF complex, which is characterized by more open entrance to the active site compared to that of hTS-dUMP-THF. Example distances in the average structures between the Cα atoms of two residues on the opposite sites of the entrance, Ser 120 and Gly 52, are 10.2 Å for hTS-dUMP-THF, 12.5 Å for (phos)hTS-dUMP-THF, and 17.7 Å for hTS-dUMP-Tomudex. In the both binary complexes, hTS-dUMP and (phos)hTS-dUMP, those distances are of the same order, and the entrances are open similarly wide, as in the (phos)hTS-dUMP-THF complex. It is noteworthy to mention that, in contrast to the protein, the ligands, dUMP and THF, experience considerable enhancement of the dynamics upon phosphorylation, observed in both the binary and ternary complexes (not shown in Fig. 4A–D). The changes in the binding positions of the ligands as a result of phosphorylation on Ser 124 will be discussed in detail further in this article.

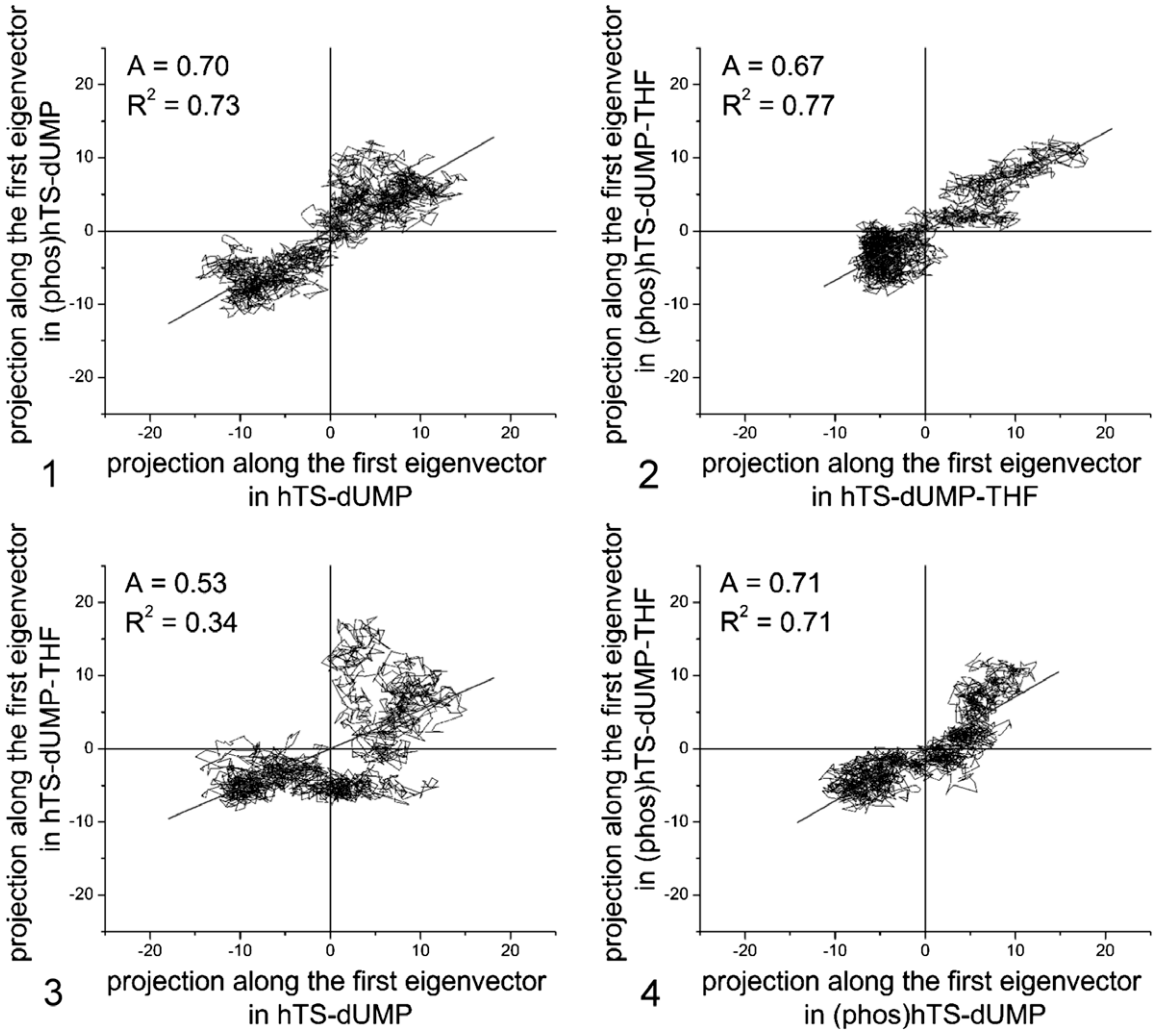

Figure 3. Time development of the projections of data collection trajectories along the first eigenvector (Å) plotted against each other in the hTS-dUMP versus (phos)hTS-dUMP (1), hTS-dUMP-THF versus (phos)hTS-dUMP-THF (2), hTS-dUMP versus hTS-dUMP-THF (3) and (phos)hTS-dUMP versus (phos)hTS-dUMP-THF (4) pairs. *A* and R^2 are the linear regression and correlation (*r* squared) coefficients, respectively.

2.3. Average structures

Average structures have been calculated by averaging coordinates from stable parts of the data collection trajectories (see Methods and Results and discussion: RMSD and RMSF). The backbone RMSD of the overall average structures with respect to the crystal structure of the hTS-dUMP-Tomudex complex, as well as the corresponding RMSD, fitted to residues composing the active sites, or to the molecule of dUMP (present in all investigated complexes), are listed in Table 2. These data show that phosphorylation affects differently the overall structures compared to the residues in the active sites or the dUMP molecule. In the case of the binary systems, the effect is similar: both the entire enzyme, the active site and dUMP show larger RMS deviations from the crystal structure in the phosphorylated than in the native complex. In the ternary systems, however, the situation is different: the RMS deviations are smaller for the entire enzyme, whereas larger for the amino acid residues in the active site or the dUMP molecule, in the phosphorylated compared to the native complex. It means that, regardless of the effect on the overall structures, the RMS deviations within the active sites were larger in the phosphorylated state compared to native systems. The latter observation corresponds to the ED results showing a strong enhancement in the motions of the ligands bound to the active sites of the phosphorylated enzymes.

In Figure 5, the average structures of the native systems are shown superimposed with structures corresponding to phosphorylated systems, and with the crystal structure of the hTS-dUMP-Tomudex complex. Figure 5 shows considerable differences in the positions of the ligands. The dUMP molecules in the hTS-dUMP and hTS-dUMP-Tomudex complexes are bound to the same site, with the pyrimidine ring in the former complex located parallel to that in the latter. Such orientation preserves configuration required for efficient binding of the cofactor (Fig. 5A). In the (phos)hTS-dUMP complex, the dUMP molecule is bound differently, with its pyrimidine, ribose and phosphate moieties shifted by about 2.5, 1.4 and 1.5 Å, respectively, relative to their positions in hTS-dUMP. In addition, the pyrimidine ring is rotated by about 25° with respect to its positions in hTS-dUMP and hTS-dUMP-Tomudex, resulting in a loss of correct orientation. Orientation (and recognition) of the pyrimidine ring in dUMP has been shown to depend strongly on the presence of the hydrogen bonds between the pyrimidine O(4) and N(3)–H moieties and the conserved active site asparagine (Asn 226 in hTS).[11,12] Therefore, the lack of correct orientation of the dUMP pyrimidine ring in (phos)hTS-dUMP can be attributed to a low occurrence of the O(4)–Asn 226 H-bond, as found from a corresponding H-bond occupancy rate of 11.3% (compared to 90.5% in hTS-dUMP) in the data collection trajectories (Table 3). In the average structure of the (phos)hTS-

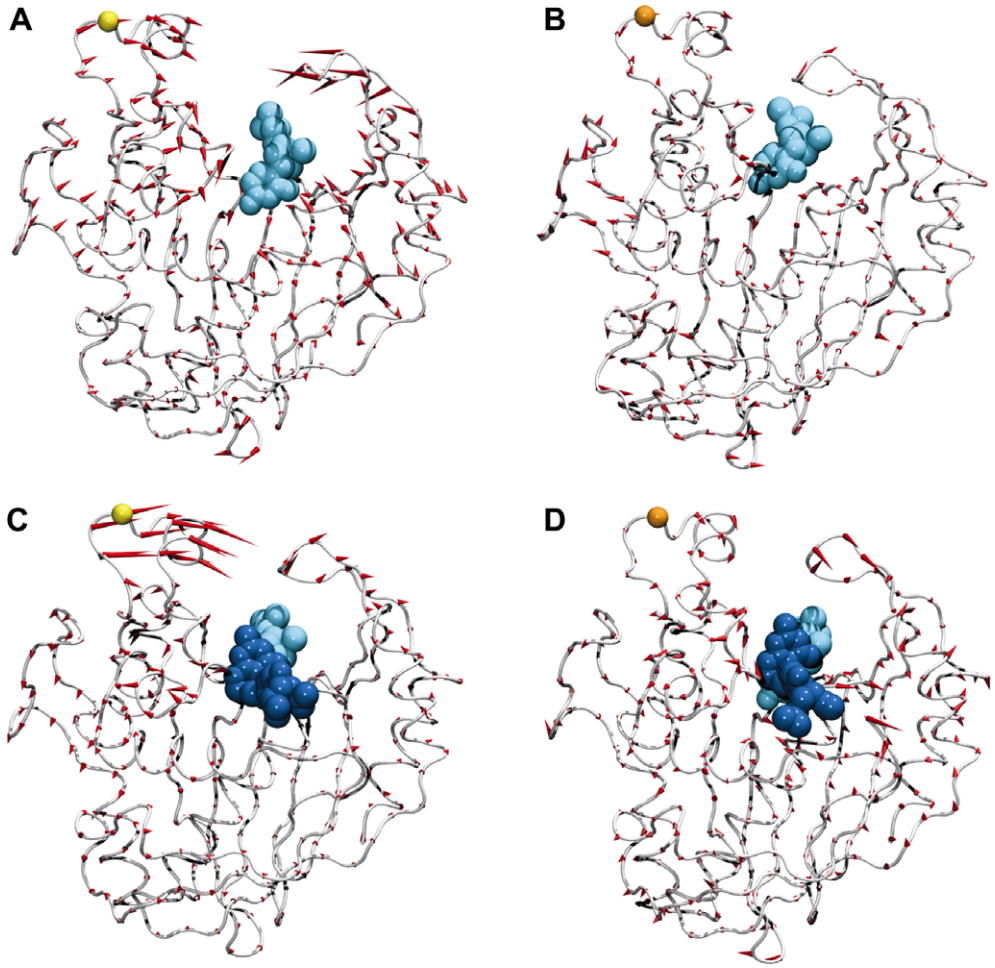

Figure 4. PORCUPINE plots of collective motions associated with the first eigenvector in hTS-dUMP (A), (phos)hTS-dUMP (B), hTS-dUMP-THF (C) and (phos)hTS-dUMP-THF (D). dUMP and THF are shown as light blue and blue spheres, respectively. Ser 124 is shown as a yellow (native systems) or orange ((phos) systems) sphere. Collective motions are shown as red cones representing the product of the first eigenvector and the first eigenvalue.

Table 2
Backbone RMSD (Å) with respect to the crystal structure of the hTS-dUMP-Tomudex complex

Complex	RMSD		
	Overall structure	Active site	dUMP
hTS-dUMP	0.91	1.16	0.39
(phos)hTS-dUMP	1.65	1.76	0.85
hTS-dUMP-THF	1.64	1.05	0.36
(phos)hTS-dUMP-THF	1.27	1.44	0.45

dUMP complex, the shift and rotation of the pyrimidine ring results in the loss of the O(4)–Asn 226 H-bond. Instead, the O(4) atom is located at an H-bond distance to the hydroxyl moiety of Tyr 135 (Fig. 5A; confirmed by a 74.7% H-bond occupancy in the trajectory). A similar drop in occurrence can be observed for H-bond between the pyridine O(2) and the amide nitrogen of Asp 218, occupied at a low rate of 10.7% (compared to 64.8% in hTS-dUMP), but not quite for the N(3)–H–Asn 226 H-bond, occupied at 57.8% (compared to 89.0% in hTS-dUMP) and observed in the average structure.

The position of the dUMP molecules and, in particular the pyrimidine rings, is similar in the pairs of average structures obtained in molecular dynamics simulations for: (i) hTS-dUMP and hTS-dUMP-THF, and (ii) (phos)hTS-dUMP and (phos)hTS-dUMP-THF. In the hTS-dUMP-THF system, strong occupancies for the O(4)–Asn 226 and N(3)–H–Asn 226 H-bonds (97.4% and 92.7%, respectively) support the correct orientation of the pyrimidine ring, whose position in the average structure is shifted about 0.6 Å in the plane of the pyrimidine ring in the crystal structure of the hTS-dUMP-Tomudex complex (Fig. 5B). The THF molecule occupies its usual binding site (which differs from that of Tomudex by a positional shift of about 3.0–3.5 Å) with the pterin ring located in close-to-parallel position with respect to the pyrimidine ring, securing favorable alignment for the catalysis. Apart from the extensive ring-stacking with dUMP, the THF position is stabilized through several hydrophobic contacts between the pterin and *p*-aminobenzoic acid (PABA) rings and the side chains of some proximal amino acid residues, including Leu 221, Phe 225, Ile 108 and Phe 80 (Fig. 6A). In the average structure of the (phos)hTS-dUMP-THF complex, the THF molecule occupies a somewhat different location, with the pterin ring shifted about 1.7 Å and slightly rotated, and the PABA ring shifted about 2.5 Å and rotated about 35°, with respect to their positions in the hTS-dUMP-THF system (Fig. 5B). Lacking most of the stacking contacts to the pyrimidine ring (only two atomic contacts within a 4 Å distance, as determined with LIGPLOT;[13] Fig. 6B), the latter molecule is stabilized via a tight hydrophobic interface connecting the PABA ring and the amino acid residues of Ile 108, Phe 225 and Leu 221, as well as via a few hydrophobic contacts between the pterin ring and the residues of Leu 192 and Trp 109. The dUMP molecule is located (in (phos)hTS-dUMP-THF) similarly as in the (phos)hTS-dUMP system, having the pyrimidine ring rotated about 30° relative to its

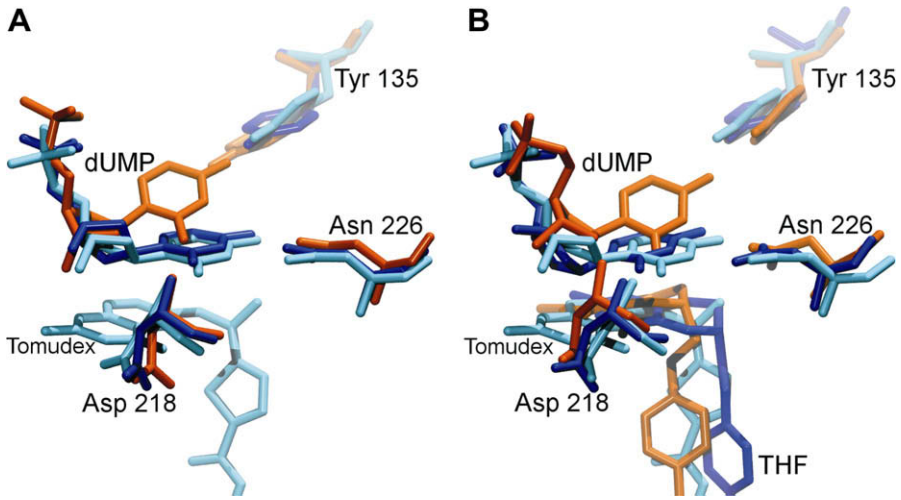

Figure 5. Superimpositions of the crystal structure of hTS-dUMP-Tomudex (light blue) and (i) the average structures of hTS-dUMP (blue) and (phos)hTS-dUMP (orange) (A), and (ii) the average structures of hTS-dUMP-THF (blue) and (phos)hTS-dUMP-THF (orange) (B). Shown are the active site residues forming hydrogen bonds with the pyrimidine ring of dUMP (Asp 218, Asn 226, Tyr 135), dUMP and THF. Hydrogen atoms are omitted for better clarity. The figure was prepared with VMD.[33]

Table 3
Hydrogen bond occupancies (%) of the atoms in the pyrimidine ring of dUMP in the data collection phases of MD simulations

Complex	Hydrogen bond occupancies			
	O(2)–Asp 218	N(3)-H–Asn 226	O(4)–Asn 226	O(4)–Tyr 135
hTS-dUMP	64.8	89.0	90.5	5.0
(phos)hTS-dUMP	10.7	57.8	11.3	74.7
hTS-dUMP-THF	64.9	92.7	97.4	0.3
(phos)hTS-dUMP-THF	0.4	75.7	0.4	99.3

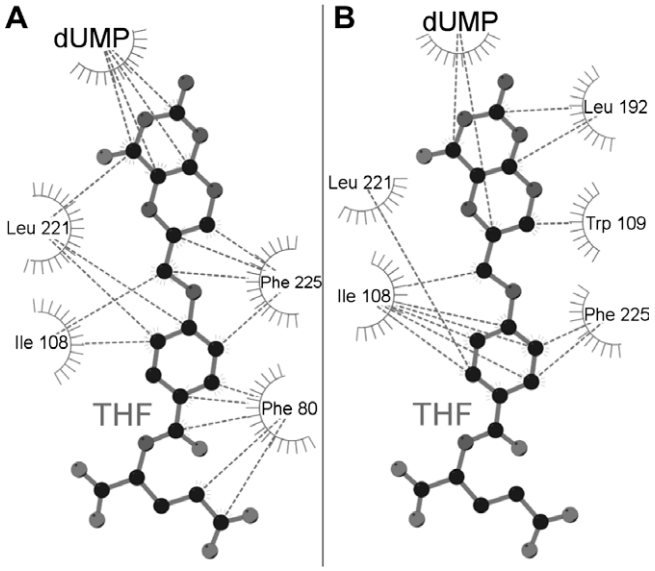

Figure 6. LIGPLOT drawings of the hydrophobic interactions THF-dUMP and THF-protein in hTS-dUMP-THF (A) and (phos)hTS-dUMP-THF (B). Hydrogen atoms in THF are omitted for clarity.

positions in hTS-dUMP-Tomudex and hTS-dUMP-THF. The N(3)–H–Asn 226 H-bond is occupied more consistently throughout the simulation (at a rate of 75.7%) than it is in (phos)hTS-dUMP, and is also present in the average structure. The O(4) atom lacks the H-bond with Asn 226, having it permanently replaced with the H-bond with Tyr 135 (as indicated by respective H-bond occupancies of 0.4% and 99.3%); likewise, the O(2) atom lacks an usual H-bond with Asp 218 (0.4% occupancy). The phosphate moiety occupies a similar but slightly shifted position with respect to that in the native ternary system, preserving all hydrogen contacts anchoring the molecule of dUMP in the active site (not shown). In the result of the altered orientation of dUMP, the alignment between dUMP pyrimidine and THF pterin rings in (phos)hTS-dUMP-THF strongly deviates from parallel, preventing from establishing the stabilizing ring-stacking interaction and being unfavorable with respect to TS catalysis. Likewise importantly, the side chain of the catalytic Cys 195 is no longer facing toward the pyrimidine ring (as is found in the hTS-dUMP-Tomudex and hTS-dUMP-THF complexes). It results in the increase of the γS (Cys 195)–C(6) (dUMP) distance from about 3.4 and 3.6 Å in hTS-dUMP-Tomudex and hTS-dUMP-THF, respectively, to about 5.3 Å in (phos)hTS-dUMP-THF. This effect renders the formation of respective thiol adduct much less expected in the phosphorylated state than in the native system.

2.4. Propagation of the 'phosphorylation effect'

In the crystal structure of the hTS-dUMP-Tomudex complex, the phosphorus atom in the phosphate moiety of dUMP and the Cα atom of Ser 124 are located at a distance of about 16.7 Å from each other. The distance increases only slightly (to ~18.1 Å) in the average structure of the hTS-dUMP-THF system, while it changes significantly (to ~23.7 Å) in the average structure of the (phos)hTS-dUMP-THF system, resulting in a large difference of about 5.6 Å between both systems. A similar effect, although less pronounced, can be observed in the average structures of the binary systems. In this case the phosphorylated Ser 124 and the phosphate moiety of dUMP are shifted by about 1 Å away from each other, compared to their respective positions in the native complex. The effect seems to originate from a long-range electrostatic repulsion between the double negatively charged phosphate moieties in dUMP and on Ser 124. The much less pronounced emergence of the effect in the binary systems may be explained by considering the more open conformation of hTS-dUMP relative to hTS-dUMP-THF (cf. ED results), with the Ser 124 Cα and dUMP phosphate separated from each other by about 3.4 Å farther in the former compared to the latter complex. The effect has severe consequences on the binding of ligands (Fig. 7). The sites of Ser 124 and dUMP are linked by a 10-amino-acid fragment 125–134

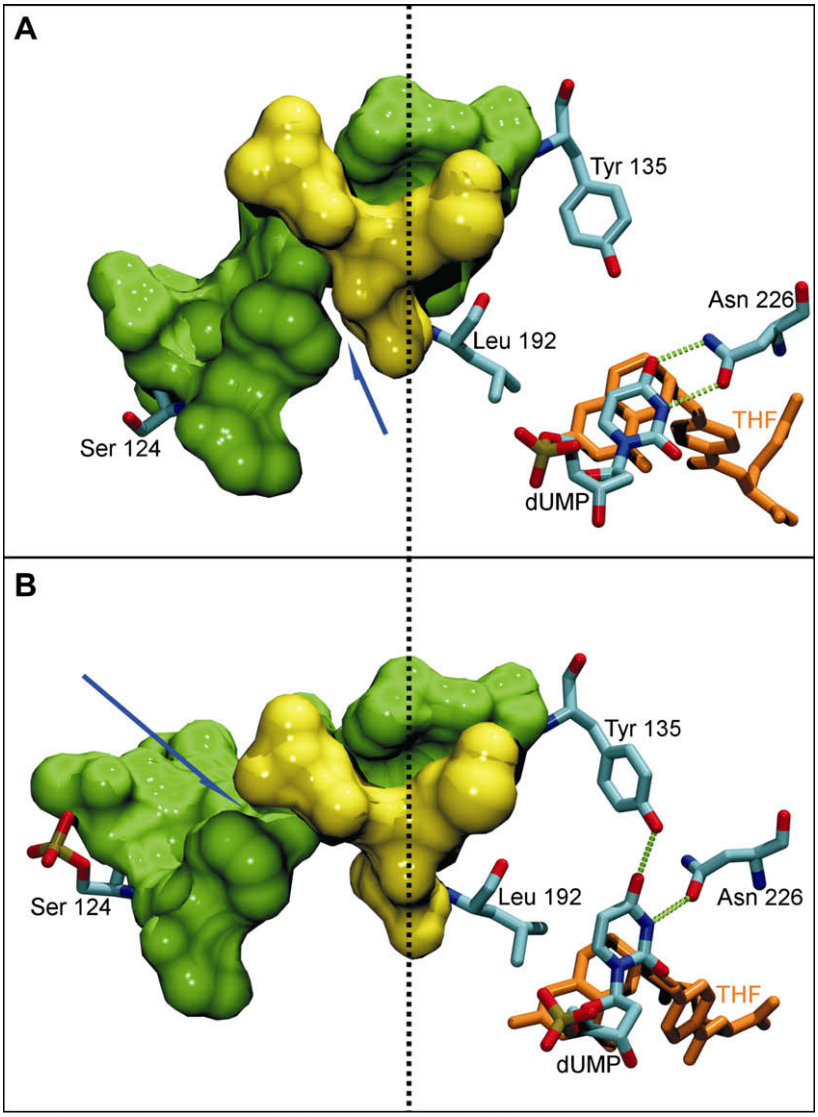

Figure 7. Transmission of the 'phosphorylation effect' from Ser 124 to the active site of human thymidylate synthase. Shown are the surface representations of the link (residues 121–134; colored green) and the patch (residues (189–192; colored yellow), and the stick representations of dUMP, THF and key amino acid residues (Ser 124, Leu 192, Tyr 135, Asn 226) in the hTS-dUMP-THF (A; native) and (phos)hTS-dUMP-THF (B; phosphorylated) complexes. The blue arrows denote hydrophobic interactions modulating the positional equilibrium between the link and the patch. Hydrogen bonds are denoted by green dotted lines. The vertical reference line is added for clearer visualization of the differences between native and phosphorylated enzymes. The figure was prepared with VMD.[33]

(the link), which is a part of the longer surface loop 121–134 connecting the two short α-helices, 115–120 and 135–140, and the helical Tyr 135, whose side chain sticks out toward the pyrimidine ring of dUMP. A short hydrophobic patch consisting of residues 189–192 plays a role of switch, transmitting the internal effects in the link to Leu 192, a residue with controlled side chain access to the ligands. In the hTS-dUMP-THF system, the link (colored green) remains in a 'compact' form, holding Tyr 135 at a distance precluding hydrogen bonding with the pyrimidine O(4) of dUMP. The patch (colored yellow) holds back Leu 192, preventing it from direct access to the ligands. In the (phos)hTS-dUMP-THF system, the Ser 124 is forced to move away due electrostatic phosphate–phosphate repulsion with dUMP, and pulls away the residues in the link, extending it by nearly 1 Å and rotating by about 18°. The movement of the link induces corresponding change in the patch, pushing Leu 192 about 2 Å toward inside of the active site, where its hydrophobic side chain contacts both the pterin ring of THF and the pyrimidine ring of dUMP, enforcing a change in the orientation of the latter ring. The latter change is coupled with a change in the H-bonding equilibrium of the O(4) atom, losing the H-bond with Asn 226 while forming the new one with Tyr 135, the phenolic ring of which is moved slightly closer and rotated for better fit. The involved mechanism depends on a positional equilibrium between the link and the patch, which seems to be modulated through the relocation of the hydrophobic bonding between Leu 121 and Phe 123 from the Ser 124 loop and Leu 189 and Ala 191 from the patch. In terms of RMSD, the change in the positions of the backbone atoms in the link and the patch equals to 1.34 and 2.34 Å for the average structures of (phos)hTS-dUMP with respect to hTS-dUMP and (phos)hTS-dUMP-THF with respect to hTS-dUMP-THF, respectively.

2.5. Free energies of binding

Free energies of binding (ΔG_{bind}) were calculated using the ensembles of structures collected along the trajectories of data collection simulations (Table 4). The results include the free energies of binding of dUMP in both binary and ternary complexes, and THF

Table 4
Free energy terms (kcal/mol) in the calculation of binding free energies in the binary and ternary complexes (values in parentheses are standard deviations)

Complex		ΔE_{ele}	ΔE_{vdW}	ΔG_{GB}	ΔG_{np}	$\Delta G_{GB,ele}$	ΔG_{bind}
hTS-dUMP		−165.29 (42.37)	−25.61 (4.33)	158.24 (38.14)	−4.56 (0.23)	−7.05 (6.34)	−37.22 (6.80)
(phos)hTS-dUMP		−77.02 (24.66)	−29.37 (3.97)	75.77 (21.33)	−4.48 (0.14)	−1.25 (5.88)	−35.10 (5.01)
hTS-dUMP-THF	dUMP	−98.79 (18.51)	−33.07 (3.63)	92.75 (16.41)	−4.46 (0.12)	−6.04 (5.26)	−43.57 (3.77)
	THF	−46.20 (26.29)	−45.95 (2.57)	67.76 (25.25)	−5.96 (0.28)	21.56 (3.06)	−30.35 (3.42)
(phos)hTS-dUMP-THF	dUMP	−32.87 (36.39)	−32.49 (4.15)	35.14 (31.21)	−4.56 (0.15)	2.27 (7.55)	−34.78 (6.67)
	THF	15.63 (38.85)	−42.04 (4.24)	7.79 (34.51)	−5.91 (0.39)	23.42 (6.75)	−24.54 (4.34)

ΔE_{int} are not included here, since they are equal zero in the single trajectory approach. $\Delta G_{GB,ele}$ is the sum of changes in the gas phase electrostatic energy and the polar solvation free energy, $\Delta E_{ele} + \Delta G_{GB}$.

in the ternary complexes. When comparing the binding free energies of dUMP, the binding is favored by more than 2 kcal/mol in the native binary compared to (phos) binary complex, and even considerably more, by nearly 9 kcal/mol in the native ternary compared to (phos) ternary complex. Although, due to lack of appropriate experimental data, such as dissociation constants for the studied complexes, these values can't be examined quantitatively and, in addition, the large difference of 9 kcal/mol seems likely to be overestimated, they correspond in a clear way to the lower versus higher V_{max}^{app} of the phosphorylated versus native hTS, respectively.[7] Inspection of the free energy contributions shows a similar pattern for both binary and ternary complexes: the binding of dUMP in the native complexes benefits strongly due to favorable ΔE_{ele} contribution, while the binding in the (phos) complexes profits similarly strongly but not sufficiently for compensation from relatively favorable ΔG_{GB} contribution. A reduction of about 7 kcal/mol in free energy favoring the binding of dUMP in hTS-dUMP compared to hTS-dUMP-THF comes partly from the balance of ΔE_{ele} and ΔG_{GB} terms (reported in Table 4 as $\Delta G_{GB,ele}$) and, in the amount of about 4 kcal/mol, from the more favorable ΔE_{vdW} contribution in (phos)hTS-dUMP compared to hTS-dUMP, in comparison to about equal ΔE_{vdW} contributions in hTS-dUMP-THF and (phos)hTS-dUMP-THF. The binding free energies of THF favor by nearly 6 kcal/mol the binding in the native (hTS-dUMP-THF) compared to phosphorylated ((phos)hTS-dUMP-THF) complex. Based on the free energy contributions, the binding of THF is favored in the native complex compared to its phosphorylated state by about 2 kcal/mol from the relatively favorable $\Delta G_{GB,ele}$ contribution (including, respectively, favorable compared to unfavorable ΔE_{ele} and more compared to less unfavorable ΔG_{GB}) and by remaining 4 kcal/mol from the more favorable ΔE_{vdW} contribution.

3. Conclusions

The present paper explores the structural and energetic origins of the effect of lowered catalytic activity of the human thymidylate synthase enzyme phosphorylated on serine 124. Our results indicate that phosphorylation changes the collective motions of the enzyme, consisting of the suppression of motions especially in the regions flanking the entrance to the active site. This was demonstrated by essential dynamics analysis of molecular dynamics trajectories. The analysis suggests that phosphorylation hinders transition from open to closed form of the enzyme in the complex with substrate and cofactor. The results reveal a different binding orientation of the pyrimidine ring of dUMP, and incorrect alignment between the pyrimidine ring and the pterin ring of THF, in the phosphorylated state compared to native hTS complexes. In the (phos)hTS-dUMP-THF complex, C(6) of the pyrimidine ring of dUMP and γS of the catalytic Cys 195 are separated by 1.7 Å further than in hTS-dUMP-THF, suggesting that formation of the thiol adduct to C(6) could be less expected. Calculated binding free energies of dUMP and THF support those findings, clearly demonstrating that both ligands bind more favorably to the native than to phosphorylated enzyme. All the results presented here offer a convincing and coherent explanation for the lowered activity of the phosphorylated enzyme. Moreover, the results suggest that phosphorylation could reduce the activity of the hTS enzyme very strong, which supports the reasoning proposed by Frączyk et al.[7]

We propose that the 'phosphorylation effect' is transmitted into the active site by a subtle structural mechanism inflicting the positional and rotational displacement of the pyrimidine ring of dUMP and, in turn, causing an impaired alignment between the latter ring and the pterin ring of THF. The mechanism is initiated by the long-range electrostatic repulsion between the phosphates in dUMP and on Ser 124. It depends on the positional equilibrium of the two amino acid fragments: the link (residues 125–134) and the patch (residues 189–192). We assign an important role in the mechanism to Leu 192, the last residue in the patch, penetrating the space around the ligands and enforcing the change in the orientation of the pyrimidine ring of dUMP, and Tyr 135, which stabilizes the new orientation by donating a hydrogen bond to the pyrimidine O(4) atom. All together, the mechanism provides an example of sophisticated machinery by which particular chemical 'events' may be transmitted from the surfaces down to the active sites of enzymes.

4. Methods

4.1. Molecular dynamics

A series of molecular dynamics (MD) simulations have been conducted to determine factors responsible for lower activity of the phosphorylated human thymidylate synthase ((phos)hTS). The simulations were initiated from the crystal structure of the ternary complex of hTS with dUMP and Tomudex (PDB accession code 1I00),[8] from which the residue numbering was also adopted. Crystallographic water molecules were discarded. Hydrogen atom positions were generated using the LEAP module of the AMBER 8 molecular modeling package.[14] The Tomudex molecule was either (i) removed, resulting in the binary system (hTS-dUMP), or (ii) replaced by the molecule of tetrahydrofolate (THF; close analogue of meTHF), resulting in the ternary system (hTS-dUMP-THF). The position of THF upon the replacement in the ternary complex resulted from the superpositioning of the crystal structures of hTS in complex with dUMP and Tomudex and *Escherichia coli* TS in complex with dUMP and THF (PDB accession code 1KZI).[15] The superimposition was performed using the least-squares fitting over skeletal atoms of the pyrimidine and sugar rings in dUMP. The phosphate group in dUMP and the carboxylic groups in THF were kept deprotonated. The Ser 124 in hTS was substituted on the hydroxyl oxygen atom with the deprotonated phosphate group, leading to phosphorylated variants of the binary and ternary systems. The native and phosphorylated systems were solvated in truncated octahedron boxes of TIP3P water molecules,[16] and periodic boundary conditions were applied during simulations. Sodium counterions were added to neutralize the net charges of the protein and li-

gands, resulting in the total number of between 20973 and 21532 atoms (depending on system). All simulations were performed using the Duan et al. (ff03) force field[17] and the SANDER module of AMBER 8. The partial atomic charges in dUMP and THF were obtained with the RESP method[18,19] by fitting the electrostatic potentials calculated at the RHF/6-31G* level of theory.

Energy minimizations were carried out using the steepest-descent and conjugate-gradient methods, followed by gradual heating to 300 K in three 7 ps intervals (0 K→100 K, 100 K→200 K, 200 K→300 K), equilibrations for 199 ps, and data collection runs for 2000 ps. The NpT ensemble (conserved number of atoms, pressure and temperature) was used throughout the simulations runs. The temperature and pressure were set to 300 K and 1 atm, respectively, with a coupling time of 1 ps for each parameter. The weak-coupling algorithm[20] and isotropic position scaling were used to monitor the temperature and pressure, respectively. A 1 fs time step and the SHAKE algorithm[21] with a relative tolerance of 0.00001 Å to constrain bonds involving hydrogen were used. Lennard–Jones and electrostatic interactions were calculated using the particle-mesh Ewald (PME) method.[22,23] The PME charge grid spacing was approximately 0.90 Å, and the charge grid was interpolated using a cubic β-spline of the order of 4 with the direct sum tolerance of 0.00001 at the 8 Å direct space cutoff. During data collection runs the coordinates were saved every 1 ps for further analysis, yielding 2000 frames for each run. Trajectories were analyzed using the PTRAJ module of AMBER 8. The behavior of the systems was monitored during the course of simulations by computing the root-mean-square-deviations (RMSD) of the backbone atoms (N, C, CA, O) of the protein. The root-mean-square-fluctuations (RMSF) of the backbone atoms were calculated to assess per-residue fluctuations in the protein. The occurrence of hydrogen bonding was evaluated using the donor–acceptor distance and donor-hydrogen-acceptor angle cutoffs of 3.2 Å and 120°, respectively. Average structures from the trajectories were calculated by stripping water and counterions, time-averaging the positions of the protein and ligands over the last 1200 ps of the data collection runs, and minimizing the average coordinates to ensure reasonable local geometries.

4.2. Essential dynamics

The trajectories from data collection runs were further analyzed using the essential dynamics technique[24,25] implemented in the PCAZIP Utilities 3.1s Principal Component Analysis-based trajectory compression and analysis toolkit.[26] Essential dynamics allows identifying essential degrees of freedom in the motion of the system. The analysis consists in the construction of the covariance matrix of the coordinate fluctuations. The covariance matrix is diagonalized to obtain the eigenvectors and eigenvalues that represent the collective (concerted) motions in the system. The eigenvectors indicate the directions of motion and the corresponding eigenvalues the amplitudes of motion along these directions. Eigenvectors with large eigenvalues, called the principal components, are considered the ones representing functionally important motions in the system. In the present work, the covariance matrices for each binary and ternary system were defined using the Cα atoms of the protein. The plots of concerted motions are prepared with the PORCUPINE program.[27]

4.3. Free energy computations

For each binary and ternary complex binding free energies of ligands to TS were computed using the Molecular Mechanics-Generalized Born Surface Area (MM-GBSA) approach.[28] The free energy of binding can be calculated according to the equation $\Delta G_{bind} = \Delta E_{mm} + \Delta G_{solv} - T\Delta S_{solute}$, where ΔE_{mm} is the molecular mechanics (MM) contribution to the binding expressed as the sum of changes in the electrostatic, van der Waals and internal energies in the gas phase ($\Delta E_{mm} = \Delta E_{ele} + \Delta E_{vdW} + \Delta E_{int}$, respectively), ΔG_{solv} is the solvation free energy contribution to binding expressed as the sum of changes in the polar and non-polar solvation free energies ($\Delta G_{solv} = \Delta G_{GB} + \Delta G_{np}$, respectively), and $T\Delta S_{solute}$ is the contribution to binding from the change in the solute entropy. After discarding water and counterions, MM energies for the complex, receptor and ligand were calculated with SANDER using a dielectric constant of 1 and an infinite cutoff for all interactions. Solvation free energies for the complex, receptor and ligand were calculated using a continuum representation of the solvent and the pairwise generalized Born (GB) model of Tsui and Case[29,30] as implemented in SANDER. Dielectric constants of 1 and 80 were assigned to the solute and solvent, respectively. Atomic radii and charges were the same as used in the MD simulations. Non-polar solvation free energies for the complex, receptor and ligand were estimated from the solvent accessible surface area (SASA) with the LCPO method[31] implemented in SANDER using the equation: $G_{np} = \gamma SASA + b$, where $\gamma = 0.0072$ kcal/(mol Å^2) and $b = 0$ kcal/mol. The solute entropy contributions to the binding free energy were not calculated in this work due to excessive computational cost of the normal mode analysis of harmonic frequencies for large systems. This methodology is often used for studying binding free energies; however, it provides only rough estimates with large margins of error.[32]

Acknowledgements

Part of the computations were performed at the Interdisciplinary Centre for Mathematical and Computational Modelling (ICM) of the Warsaw University, Poland.

References and notes

1. Carreras, C.; Santi, D. V. *Annu. Rev. Biochem.* **1995**, *64*, 721.
2. Costi, M. P.; Ferrari, S.; Venturelli, A.; Calò, S.; Tondi, D.; Barlocco, D. *Curr. Med. Chem.* **2005**, *12*, 2241.
3. Gmeiner, W. H. *Curr. Med. Chem.* **2005**, *12*, 191.
4. Liu, J.; Schmitz, J. C.; Lin, X.; Tai, N.; Yan, W.; Farrell, M.; Bailly, M.; Chen, T.; Chu, E. *Biochim. Biophys. Acta* **2002**, *1587*, 174.
5. Rahman, L.; Voeller, D.; Rahman, M.; Lipkowitz, S.; Allegra, C.; Barrett, J. C.; Kaye, F. J.; Zajac-Kaye, M. *Cancer Cells* **2004**, *5*, 341.
6. Litchfield, D. W. *Biochem. J.* **2003**, *369*, 1.
7. Frączyk, T.; Kubiński, K.; Masłyk, M.; Cieśla, J.; Hellman, U.; Shugar, D.; Rode, W. *Bioorg. Chem.* **2010**, *38*, 124.
8. Almog, R.; Waddling, C. A.; Maley, F.; Maley, G. F.; Van Roey, P. *Protein Sci.* **2001**, *10*, 988.
9. Perry, K. M.; Carreras, C. W.; Chang, L. C.; Santi, D. V.; Stroud, R. M. *Biochemistry* **1993**, *32*, 7116.
10. Stroud, R. M.; Finer-Moore, J. S. *Biochemistry* **2003**, *42*, 239.
11. Finer-Moore, J. S.; Liu, L.; Schafmeister, C. E.; Birdsall, D. L.; Mau, T.; Santi, D. V.; Stroud, R. M. *Biochemistry* **1996**, *35*, 5125.
12. Liu, L.; Santi, D. V. *Biochemistry* **1993**, *32*, 9263.
13. Wallace, A. C.; Laskowski, R. A.; Thornton, J. M. *Protein Eng.* **1995**, *8*, 127.
14. Case, D. A.; Darden, T. A.; Cheatham, T. E., III; Simmerling, C. L.; Wang, J.; Duke, R. E.; Luo, R.; Merz, K. M.; Wang, B.; Pearlman, D. A.; Crowley, M.; Brozell, S.; Tsui, V.; Gohlke, H.; Mongan, J.; Hornak, V.; Cui, G.; Beroza, P.; Schafmeister, C.; Caldwell, J. W.; Ross, W. S.; Kollman, P. A. AMBER 8, University of California: San Francisco, 2004.
15. Fritz, T. A.; Liu, L.; Finer-Moore, J. S.; Stroud, R. M. *Biochemistry* **2002**, *41*, 7021.
16. Jorgensen, W. L. *J. Chem. Phys.* **1982**, *77*, 5757.
17. Duan, Y.; Wu, C.; Chowdhury, S.; Lee, M. C.; Xiong, G.; Zhang, W.; Yang, R.; Cieplak, P.; Luo, R.; Lee, T. *J. Comput. Chem.* **2003**, *24*, 1999.
18. Bayly, C. I.; Cieplak, P.; Cornell, W. D.; Kollman, P. A. *J. Phys. Chem.* **1993**, *97*, 10269.
19. Cieplak, P.; Bayly, C. I.; Cornell, W. D.; Kollman, P. A. *J. Comput. Chem.* **1995**, *16*, 1357.
20. Berendsen, H. J. C.; Postma, J. P. M.; van Gunsteren, W. F.; DiNola, A.; Haak, J. R. *J. Chem. Phys.* **1984**, *81*, 3684.
21. Ryckaert, J. P.; Ciccotti, G.; Berendsen, H. J. C. *J. Comput. Phys.* **1977**, *23*, 327.
22. Essmann, U.; Perera, L.; Berkowitz, M. L.; Darden, T.; Lee, H.; Pedersen, L. G. *J. Chem. Phys.* **1995**, *103*, 8577.
23. York, D. M.; Darden, T. A.; Pedersen, L. G. *J. Chem. Phys.* **1993**, *99*, 8345.
24. Amadei, A.; Linssen, A. B.; Berendsen, H. J. C. *J. Biomol. Struct. Dyn.* **1993**, *17*, 412.

25. Amadei, A.; Linssen, A. B.; de Groot, B. L.; van Aalten, D. M.; Berendsen, H. J. C. *J. Biomol. Struct. Dyn.* **1996**, *13*, 615.
26. Meyer, T.; Ferrer-Costa, C.; Perez, A.; Rueda, M.; Bidon-Chanal, A.; Luque, F. J.; Laughton, C. A.; Orozco, M. *J. Chem. Theory Comput.* **2006**, *2*, 251.
27. Haider, S.; Parkinson, G. N.; Neidle, S. *Biophys. J.* **2008**, *95*, 296.
28. Kollman, P. A.; Massova, I.; Reyes, C.; Kuhn, B.; Huo, S.; Chong, L.; Lee, M.; Lee, T.; Duan, Y.; Wang, W.; Donini, O.; Cieplak, P.; Srinivasan, J.; Case, D. A.; Cheatham, T. E., III *Acc. Chem. Res.* **2000**, *33*, 889.
29. Tsui, V.; Case, D. A. *Biopolymers* **2001**, *56*, 275.
30. Tsui, V.; Case, D. A. *J. Am. Chem. Soc.* **2000**, *122*, 2489.
31. Weiser, J.; Shenkin, P. S.; Still, W. C. *J. Comput. Chem.* **1999**, *20*, 217.
32. Weis, A.; Katebzadeh, K.; Soderhjelm, P.; Nilsson, I.; Ryde, U. *J. Med. Chem.* **2006**, *49*, 6596.
33. Humphrey, W.; Dalke, A.; Schulten, K. *J. Mol. Graph.* **1996**, *14*, 33.